JET-P(95)07

Radial and Poloidal $\vec{E}\times B$ $\vec{D}$rifts in the Scrape-off Layers of a Divertor Tokamak: Effects on In/Out Asymmetries, Plasma Detachment at the Targets, and Divertor Biasing

P C Stangeby[1], A V Chankin[2].

JET Joint Undertaking, Abingdon, Oxfordshire, OX14 3EA, UK.
[1] University of Toronto Institute for Aerospace Studies, Ontario, Canada, M3H 5T6.
[2] Permanent address: INF Russian Scientific Centre "Kurchatov Institute", Institute for Nuclear Fusion, Moscow, Russia.

Preprint of a paper to be submitted for publication in Nuclear Fusion

April 1995

ABSTRACT

The influence of radial and poloidal E×B drifts in the Scrape-Off Layer of a divertor tokamak are considered. For $\vec{B}$ in the "forward" direction (the $\vec{\nabla}B$ ion drift toward a lower X-point, single null divertor configuration), the poloidal drift tends to increase the plasma pressure and the recycling rates at the outer target, lowering the temperature there – as compared with the inner target. When the radial drift dominates, these asymmetries are reversed. The radial drift is estimated to be more important than the poloidal drift for high $\bar{n}_e$-operation (the "high recycling" regime). Poloidal drifts can result in substantially reduced plasma contact at one target ("detachment"); simultaneous detachment at both targets due to poloidal drifts appears to be less likely. Radial drifts could result in detachment at one or both targets, but the type of detachment involved does not appear to be consistent with that experimentally observed. The experimental observations made in the Tokamak de Varennes, with divertor biasing arranged to increase/decrease the radial electric field in the SOL, relative to its natural level, are broadly consistent with the poloidal drift model.

1. INTRODUCTION

The region outboard of the Last Closed (Magnetic) Flux Surface, LCFS, in a magnetically confined plasma device, such as a tokamak, is called the Scrape-Off Layer, SOL, and is generally characterized by strong plasma flows. These flows virtually always include motion along $\vec{B}$, but can also include flows cross-field – the so-called "drifts" (there are also cross-field diffusive or turbulent fluxes but these are not the focus of this paper). The parallel-to-$\vec{B}$ flows are, in the simplest cases, due to the fact that the particle sources in the SOL – whether from local ionization of neutrals, or due to cross-field diffusion from ionization sources inside the LCFS – are located some distance from the particle sinks, i.e., the limiters or divertor target plates, and the flow arises to connect source and sink.

It is almost inevitable that radial and poloidal gradients of electric potential and plasma potential will arise naturally in the SOL – even without any external biasing. These gradients then cause radial and poloidal diamagnetic and $\vec{E}\times\vec{B}$ drifts:

$$\vec{v}_{\vec{E}\times\vec{B}} = \frac{\vec{E}\times\vec{B}}{B^2} \tag{1}$$

$$\vec{v}_{\vec{\nabla}p} = \frac{\vec{B}\times\vec{\nabla}p}{n_e B^2} \tag{2}$$

Diamagnetic drifts are largely divergence-free and therefore do not contribute to the fluxes to external surfaces such as divertor plates, nor do they deposit plasma in any local volume of the plasma. (Only "largely" divergence-free: in a toroidal system, part of the diamagnetic drift gives the $\vec{\nabla}B$ drift which does result in net up/down transport.) These diamagnetic drifts are discussed further in [1]. They will not be considered further here.

Radial electric fields exist naturally in the SOL due to various causes. The simplest cause is related to the general use of electrically conducting target plates, defining a natural reference value of the electric potential $\phi=0$. The electron temperature $T_e(r)$ generally decreases radially in the SOL since the heat source is inboard of the LCFS. The potential drop across the Debye sheath (or combined Debye and magnetic pre-sheath) at the target is ~3 $T_e(r)/e$, assuming hydrogenic ions, and locally ambipolar (electron outflux = ion outflux) conditions. Thus, in this simplest case one has:

$$\phi(r) = \frac{3T_e(r)}{e} \tag{3}$$

and so the radial electric field:

$$E_r \equiv\approx -\frac{\partial\phi}{dr} \approx -\frac{3T_e}{e\ell_{T_e}}\left(=\frac{3T_e}{e\lambda_{T_e}}\right) \tag{4}$$

where $$\ell_{T_e} \equiv \left(\frac{1}{T_e}\frac{\partial T_e}{\partial r}\right)^{-1},$$

the characteristic length of radial variation in the SOL. If $T_e(r)$ decays exponentially – often a good approximation – then $\ell_{T_e} \equiv -\lambda_{T_e}$ is the e-folding length. In this latter case, E_r points radially outward. Therefore if $\vec{B}$ is in the "forward" direction (the $\vec{\nabla}B$-ion drift is toward the lower x-point of a single-null divertor configuration), Fig. 1, then the poloidal drift velocity v_{pol}, is directed toward the outer target within the SOL. (In the Private Plasma, at the outside target, v_{pol} would be away from the target, assuming T_e decays radially going into the Private Plasma.)

This poloidal drift can change the parallel flow velocity associated with connecting the particle source and sink at the targets (boundary conditions on $v_{\|}$ at the Entrance to the Magnetic Pre-sheath) [2]. In Section 3 the consequences of this effect are considered on in/out asymmetries at the two targets of a single-null divertor tokamak.

It is also generally the case that an electric field will exist along $\vec{B}$ in the SOL, giving a poloidal electric field E_{pol}, and thus radial $\vec{E}\times\vec{B}$ drifts at velocity v_r. Even if T_e does not vary along the SOL, one will have the usual $\sim\ell n2T_e/e$ drop associated with the pre-sheath acceleration of the plasma up to the acoustic speed near the target and the corresponding drop

in density. For the cases of greatest interest, strong temperature gradients exist along the SOL and the thermo-electric force gives rise to a potential drop of order T_e at the midplane which is $>>T_e$ at the target. The momentum equation for electrons along the $\vec{B}$ direction s, for a hydrogenic plasma, is:

$$-\frac{\partial p_e}{\partial s} + en\frac{\partial \phi}{\partial s} + en\frac{j}{\sigma_{||}} - 0.71n\frac{\partial T_e}{\partial s} = 0 \tag{5}$$

Assuming, for simplicity, p_e = constant and j = 0 then:

$$E_{||} \equiv -\frac{\partial \phi}{\partial s} \approx -\frac{1}{e}\frac{\partial T_e}{\partial s} \tag{6}$$

Thus, on the outside, $E_{||}$ and E_{pol} point toward the target and so $v_r = \vec{E}_{pol} \times \vec{B}/B^2$ points radially inward, Fig.1, for the "forward" direction of $\vec{B}$. In [3] such flows were considered; however, there the critical assumption was made that the pressure is constant along the SOL, which will not be assumed here since we are seeking an explanation of in/out pressure differences.

Unlike v_{pol}, v_r does not directly "compete" with $v_{||}$, the flow velocity along $\vec{B}$. In the simplest picture, this radial drift forms its own closed loop of recirculating flow, see Fig.2, where we have assumed that the recycle patterns at each target are also locally closed – i.e., the "high recycling" divertor situation (with the neutrals recycling from the outer/inner target all ionize close to the outer/inner target, creating a local plasma flow back to the outer/inner target; ionization-pattern-induced flow reversal [4-8] is excluded in this simplest picture). In this case, the flow pattern caused by v_r would consist of flow from the outer SOL, across the LCFS into the core plasma, out again across the LCFS into the inner SOL, with the circuit completed by parallel-to-$\vec{B}$ flow along the SOL over the top side of the plasma. Clearly much more complex flow patterns could arise resulting in direct interaction (i.e., co-mingling) of the v_r-flow fields and those associated with the spatial distribution of ionization. Here, however, we will only consider the simplest possible case as indicated in Fig.2. In this simplest case, if $v_r = 0$, then the entire region in the SOL, between the recycling zones localized near the two targets, would be stagnant; it is only due to $v_r \neq 0$ that there is any parallel-to-$\vec{B}$ flow in most of the SOL, for these assumptions.

In the presence of dissipative forces, such as friction or shear viscosity, the parallel flow needed to close this loop, results in parallel pressure drops along the SOL, giving in/out asymmetries. (Even without dissipative losses, there is some pressure drop along the SOL since stagnant plasma is taken in from the core, while plasma containing momentum is returned to the core [9].) This case is considered in Section 4.

2. THE RELATIVE IMPORTANCE OF POLOIDAL AND RADIAL $\vec{E}\times\vec{B}$ DRIFTS

In a full treatment of the problem, as can be done with numerical codes [10, 11], one would just include both types of $\vec{E}\times\vec{B}$ drift. For purposes of estimating drift effects, and for understanding basic trends, it is clearly advantageous if one can consider regimes where one or the other of the two drifts is dominant.

We start by considering the "low recycling" regime – or, to be more explicit, the regime where there is little temperature variation along the SOL (sometimes also called the "sheath-limited" regime). We can estimate the total poloidal flux per unit toroidal length along the SOL [12]:

$$F_{pol} \approx n_e E_r \lambda_{SOL}/B \approx n_e 3T_e/eB \tag{7}$$

This equation assumes (a) an ambipolar sheath drop of $3kT_e/e$, (b) isothermal conditions along the SOL. The total radial flux per unit toroidal length from the entire outer SOL, across the separatrix, and thence into the inner SOL is:

$$F_{rad} \approx \int_{top}^{outer\ target} E_\theta d\ell_\theta \approx n_e T_e / 2eB \tag{8}$$

where it is assumed that an isothermal, potential drop of $\frac{1}{2}kT_e/e$ exists along the SOL.

Clearly, in this regime the poloidal $\vec{E}\times\vec{B}$ drift dominates and, to first order, one can neglect the radial drift. This case is analysed in Sec. 3.

Next we consider the "high recycling" regime – or to be more explicit the regime with significant parallel temperature gradients along the SOL (sometimes also called the "conduction-limited" regime). Assuming that $T_e^{top} >> T_e^{div}$, and using Eq.(6) one might estimate that the total radial flux would now be:

$$F_{rad} \approx n_e T_e^{top} / eB \tag{9}$$

while the total poloidal flux, across the SOL, at the top, per m toroidally, would be

$$F_{pol}^{top} \approx n_e E_r^{top} \lambda_{SOL} / B \approx n_e T_e^{top} / eB \tag{10}$$

where the effect of the $3kT_e^{div}/e$ sheath drop has been ignored since $T_e^{top} >> T_e^{div}$. On the basis of such an estimate one would conclude that both drifts were equally important in this regime. This is not correct, however, because one has ignored the fact that almost certainly n_e

has *also* varied along the SOL, not just T_e, and n_e-variations were not included in these estimates. One must therefore consider this regime more carefully.

The first task is to find $\phi(r, y)$ where, in this section:

r = radial coordinate, measured from separatrix outward into the SOL,

y = poloidal coordinate, measured from inner target.

For simplicity we will assume: $j_{||} = 0$, i.e., local ambipolar sheaths, thus from Eq. (5):

$$en\frac{\partial\phi}{\partial y} = \frac{\partial p}{\partial y} + 0.71\, n\frac{\partial T}{\partial y} \tag{11}$$

For illustration one could take $\partial p/\partial y = 0$, but a more general case (yet still tractable) is easily generated which allows for the usual feature of p and T increasing with y by assuming:

$$p(r, y) = p(r, 0)\,[T(r, y)/T(r, 0)]^{\alpha} \tag{12}$$

Thus, for example, if one wanted p to increase by the usual factor of 2 (Mach number unity at the targets), and if, say, $T_{top}/T_{div} = 20$ (we will assume here that α is the same for all r) then the constant $\alpha = 0.231$. For p = constant along y, $\alpha = 0$.

This then gives:

$$e\phi(r, y) = (\alpha + 0.71)\,[T(r, y) - T(r, 0)] + 3T(r, 0) \tag{13}$$

$$\approx (\alpha + 0.71)\,T(r, y) \tag{14}$$

assuming $T(r, y) >> T(r, 0)$ and the factor 3 in Eq. (13) assumes an ambipolar sheath drop of $3kT_e/e$.

In this section, for simplicity, we take $\left|\vec{B}_{tor}\right| = 1$ tesla. Thus the total radial flux is now:

$$\begin{aligned} F_{rad} &= -\int_{y=0}^{L_{pol}} n(0,y)E_{pol}(0,y)dy \\ &= \int_0^{L_{top}} n(0,y)\frac{\partial\phi}{\partial y}(0,y)dy \\ &= (\alpha+0.71)\int_0^{L_{top}} n(0,y)\frac{\partial T(0,y)}{\partial y}dy \\ &= \left(1+\frac{0.71}{\alpha}\right)\left[\left[\frac{T(0,L_{top})}{T(0,0)}\right]^{\alpha} - 1\right]p(0,0) \end{aligned} \tag{15}$$

plus a magnetic pre-sheath component which is readily shown to be $\approx 1p(0, 0)$; see [1].

For purposes of calculating F_{pol} we assume:

$$n(r, y) = n(0, y)e^{-r/\lambda_n}$$
$$T(r, y) = T(0, y)e^{-r/\lambda_T} \tag{16}$$

And so for locations well upstream from the target, again neglecting the sheath contribution:

$$E_{radial}(r,y) \approx -(0.71+\alpha)\frac{\partial T(r,y)}{\partial r} = (0.71+\alpha)\frac{T(r,y)}{\lambda_T} \tag{17}$$

$$\therefore F_{pol}^{top} = \int_{separatrix}^{wall} E_{rad}\left(r, L_{top}\right)n\left(r, L_{top}\right)dr$$
$$= (0.71+\alpha)\left[\frac{T\left(0, L_{top}\right)}{T(0,0)}\right]^{\alpha}\frac{\lambda_p}{\lambda_T}p(0,0) \tag{18}$$

We also have: $$F_{pol}^{div} \approx 3p(0, 0)\lambda_p/\lambda_T \tag{19}$$

We may then consider the example of:

Say $$T(0, L_{top})/T(0, 0) = 20 \tag{20}$$

and $$p(0, L_{top})/p(0,0) = 2 \quad \therefore \quad \alpha = 0.231 \tag{21}$$

and $$F_{rad} = 4.07p(0, 0) + \approx 1p(0, 0) \approx 5p(0, 0) \tag{22}$$

$$F_{pol}^{top} = 0.94p(0, 0) \qquad \text{assuming } \lambda_n = \lambda_T \tag{23}$$

$$F_{pol}^{div} = 1.5p(0, 0) \qquad \text{assuming } \lambda_n = \lambda_T \tag{24}$$

so $$F_{pol}^{net\ into\ SOL} = 0.56p(0, 0) \qquad \text{assuming } \lambda_n = \lambda_T \tag{25}$$

We may then conclude, at least to the degree that this particular example is indicative of general trends for "high recycling" conditions:

(a) F_{rad} dominates all the poloidal fluxes, and to a first degree they should be ignorable.

(b) In any case, F_{pol}^{net} is in the same direction as F_{rad}, i.e., it brings plasma **into** the SOL. Thus, even the sign is in the wrong direction for conjecturing that perhaps the divergence of the radial flux could be compensated by the divergence of poloidal flux.

(c) As detached conditions are approached, $p(0, L_{top})/p(0, 0)$ increases further. Initially this makes F_{rad} still more dominant, but then it reduces again for very high pressure drop.

Nevertheless, one should also note:

(a) The foregoing is a particular illustration and may not be general. It presumably, however, indicates the trend.

(b) The radial and poloidal fluxes are certainly not **hugely** different and in a code it would be advisable to allow for both drifts simultaneously. For purposes of understanding trends and making estimates it appears, however, that it is justified to treat each drift separately.

(c) The foregoing illustration has also not allowed for the development of the parallel pressure differences which the drifts themselves create, i.e., feedback effects. It is therefore a "small signal" analysis.

(d) Even if $F_{rad} >> F_{pol}$, it is not guaranteed that this means that the pressure asymmetry caused by F_{rad} (tending to make the inner pressure higher) will overwhelm the pressure asymmetry due to F_{pol} (tending to make the outer pressure higher) – although this would seem likely. (In order to make solid quantitative comparisons one would need to quantify the viscous and frictional drag on the parallel return fluxes, see Sec. 4).

(e) Complications due to non-ambipolar sheaths and to "co-mingling" of the drift and ionization-driven flows have been neglected and would conceivably change the picture.

It seems likely, therefore, that even if there is something of these trends:

1. for "low-recycling" divertors, i.e., isothermal along $\bar{B}$, to be governed by poloidal drifts, while -
2. for "high-recycling" divertors, i.e., large parallel gradients of T and n, to be governed by radial drifts -

– there are likely to be numerous exceptions.

The case of purely radial $\vec{E}\times\vec{B}$ drift is considered in Sec. 4.

It should be noted that we have so far described only the simplest possible picture for these drifts. The value of E_r, for example, is not necessarily positive at all points in the SOL: the flow to the targets is not necessarily locally ambipolar, i.e., substantial currents can exist [13, 14]. Such currents would also influence $E_{||}$, E_θ, see Eq. (5). The sheath voltage drop is not always $\sim 3T_e/e$, even if local ambipolarity holds; secondary electron emission influences the floating sheath potential drop [15]. To deal with the full range of possibilities it is necessary to use 2D codes which solve the conservation equations for the full system, SOL plus divertor plasmas, taking into account the proper boundary conditions at the targets – including the effects of poloidal drifts [2] – and allowing for the influence of currents and drifts throughout the edge plasma [10, 11]. Here, we must by-pass such ambitious numerical analysis. We will do this by:

(a) restricting ourselves to the simplest cases, as already described, including the assumption that either radial or poloidal drifts are present, but not both simultaneously,

(b) using boundary conditions from [2], which are expressed in a general form, not assuming necessarily that the sheath potential drop is locally $\sim 3T_e/e$, nor that the electron temperature decreases radially, etc.

The conclusions we can draw from such an undertaking, therefore, can only be broad ones.

3. POLOIDAL $\vec{E}\times\vec{B}$ DRIFT

The geometry is shown in Fig. 3.

Assume that an ionization, or cross-field particle, source is specified, S_{iz}. S_{iz} can be taken to represent the net effect of ionization and recombination plus "anomalous" (presumably fluctuation-driven) cross-field sources/sinks; we explicitly exclude, however, sources/sinks associated with drifts, as we include these separately, below. Then the particle conservation equation is:

$$\frac{d}{dy}\left[n\left(\cos\theta\, v_{pol} + \sin\theta\, v_{||}\right)\right] = S_{iz} \tag{26}$$

The momentum equation in the parallel direction is:

$$mnv_{||}\frac{dv_{||}}{ds_{||}} = -\frac{dp_i}{ds_{||}} + neE_{||} + S_m - mv_{||}S_p - mv_{||}S_{iz} \tag{27}$$

where S_p and S_m are the particle and momentum "source" rates, respectively, for the parallel direction due to the divergence of the drift flow at speed v_{pol}. Viscous stress has been neglected.

For simplicity we take the isothermal approximation, thus the first two terms on the RHS of Eq. (27) become:

$$-c_s^2 m\frac{dn}{ds_{||}} \tag{28}$$

where
$$-c_s^2 = k(T_e + T_i)/m \tag{29}$$

Defining the coordinate pair $(s_{||}, s_\perp)$ in the (x, y) plane, we have:

$$dy = \cos\theta\, ds_\perp, \quad dx = \cos\theta\, ds_{||}, \text{ etc.} \tag{30}$$

Then:
$$S_p = -\frac{d}{ds_\perp}(nv_{pol}) \tag{31}$$

$$= -\cos\theta\frac{d}{dy}(nv_{pol}) \tag{32}$$

and
$$S_m = -\frac{d}{ds_\perp}(mv_{||}nv_{pol}) \tag{33}$$

therefore
$$S_m - mv_{||}S_p = -\cos\theta\, mnv_{pol}\frac{dv_{||}}{dy} \tag{34}$$

Combining (27), (28), (30) and (34) gives:

$$n\frac{dv_{||}}{dy}\left(\frac{v_{pol}}{\tan\theta} + v_{||}\right) = -c_s^2\frac{dn}{dy} - v_{||}\frac{S_{iz}}{\sin\theta} \tag{35}$$

If one treats $v_{pol}(y)$ as specified, also T_e, T_i, $S_{iz}(y)$, $\theta(y)$, then we have two equations, (26) and (35), to give the two quantities $n(y)$ and $v_{||}(y)$. It would be illuminating to solve these

differential equations for specified drifts $v_{pol}(y)$, however, here for purposes of simple estimates we assume $v_{pol}/\tan\theta$ constant along y. We thus ignore the poloidal variation of v_{pol} associated with Pfirsch-Schluter flows.

We combine the particle balance equation (26) and the momentum equation (35) to get:

$$n\frac{dv_{||}}{dy}\left(\frac{v_{pol}}{\tan\theta}+v_{||}\right)+v_{||}\frac{d}{dy}\left[n\left(\frac{v_{pol}}{\tan\theta}+v_{||}\right)\right]=-c_s^2\frac{dn}{dy} \tag{36}$$

Assuming $\left(\frac{v_{pol}}{\tan\theta}\right)$= constant allows one to replace $\frac{dv_{||}}{dy}$ by $d\left(\frac{v_{pol}}{\tan\theta}+v_{||}\right)/dy$. Also, define:

$$v \equiv v_{||}+\frac{v_{pol}}{\tan\theta} \tag{37}$$

and we can now integrate Eq. (36) to give:

$$n\left(v^2+c_s^2-\frac{v_{pol}}{\tan\theta}\right)= G, \text{ a constant} \tag{38}$$

At this point the boundary conditions are needed to specify $v_{||}$ at the Entrance to the Magnetic Pre-Sheath, MPS, in front of the target plates, $v_{||B\ MPSE}$. This is given in [2]. Results are repeated here without derivation:

$$\frac{v_{||B\ MPSE}}{c_s} \equiv M_o = -\gamma(2+a+b)+\left[\gamma^2(a+b)^2+1+4a\gamma^2\right]^{1/2} \tag{39}$$

where γ gives the normalized strength of the drift:

$$\gamma \equiv \frac{v_{pol}}{2c_s\tan\theta} \tag{40}$$

and the a, b factors are given by the radial gradients (x-direction) of the edge plasma:

$$a \equiv \frac{1}{|\psi w|}\frac{l_{sh}}{l_v} \tag{41}$$

$$b \equiv -\frac{1}{|\psi w|}\frac{l_{sh}}{l_n} \tag{42}$$

where $|\psi_w|T_e/e$ = total (normalized) potential drop across the MPS and Debye sheath (≈3 for simple cases).

Also
$$l_{sh} \equiv \left[\left(l_{T_e} \right)^{-1} + \left(l_{\psi} \right)^{-1} \right]^{-1} \tag{43}$$

$$l_n \equiv \left[\frac{1}{n_e} \frac{dn_e}{dx} \right]^{-1} \tag{44}$$

$$l_{T_e} \equiv \left[\frac{1}{T_e} \frac{dT_e}{dx} \right]^{-1} \tag{45}$$

$$l_{\psi} \equiv \left[\frac{1}{|\psi w|} \frac{d|\psi w|}{dx} \right]^{-1} \tag{46}$$

$$l_v \left[\frac{1}{v_{||}} \frac{dv_{||}}{dx} \right]^{-1} \tag{47}$$

It is only possible to establish the values of a, b by carrying out a full 2D (numerical) analysis of the entire SOL + divertor plasma + boundary condition system [10, 11]. (Indeed, iteration is needed to evaluate l_v self-consistently.) It is therefore beyond the present analysis to attempt to relate a, b to the basic parameters controlling the system (i.e., the power flow across the LCFS, the upstream/reference plasma density, the anomalous cross-field particle, momentum and heat diffusivities, secondary electron emission properties of the target, etc.). Here we will just use $M_o(\gamma, a, b)$, Eq. (39), and illustrate results by various arbitrary choices of values γ, a, b.

To a first approximation (assuming all scale lengths are ≈ same, and $|\psi_w| \approx 3$, so that a, b are small compared with unity) Eq. (39) gives the simple "intuitive" result (if a = b = 0) that:

$$M_o = 1 - 2\gamma \tag{48}$$

"Intuitive" because one derives this result by just assuming that the total velocity (vectorial sum of drift and parallel velocity) at the MPSE is the sound speed. This was the boundary condition used by Staebler [10] and in [16] by Cohen and Ryutov. The results given below are identical to those of [16] in this limit. Tendler and Rozhansky [17] have also treated this case and shown that in/out pressure differences are created by poloidal drifts; this latter work differs from the present study, however, by (a) including diamagnetic drifts, which do

not, in fact, contribute to outfluxes [1], and (b) by leaving the value of M_o unspecified. Recently, Krasheninnikov et al [18] have reformulated the problem; the latter work differs from the present study by (a) again including diamagnetic drifts, (b) including both poloidal and radial drifts simultaneously, and (c) using the Bohm Criterion in its original form, unmodified by the presence of drifts, thus $M_o = 1$.

From Eqs. (37) and (39) we have the boundary ("0") value for v:

$$v_o = c_s(2\gamma + M_o) \tag{49}$$

(= c_s for the intuitive boundary conditions)

From Eq. (38) one thus has the density just in front of the target:

$$n_o = \left(G / c_s^2\right)\left[M_o\left(M_o + 2\gamma\right) + 1\right]^{-1} \tag{50}$$

One can thus calculate the in/out density ratio, n_o^{in} / n_o^{out}, where we assume that $v_{pol}, \gamma > 0$ at the outer target, while at the inner target these quantities have the same absolute magnitude, but of opposite sign. Results are shown in Fig. 4 for $0 \leq \gamma \leq 1$ and for illustrative examples of (a, b).

For the "intuitive" boundary conditions, i.e., (a,b)=(0,0), one finds that n_o^{in} / n_o^{out} rapidly decreases for increasing v_{pol}, γ. This is also true for some of the other sets of (a, b), but for some there is no asymmetry, while for (a, b) both negative the asymmetry actually is reversed.

Here, since an isothermal approximation has been made, the pressure asymmetry is the same as the density asymmetry. Thus, usually, the pressure will be highest at the outside target, for "forward" $\vec{B}$, when poloidal E×B drifts are strong, and the recycling will be strongest there.

The *total* outflux density is given by the vectorial sum of the drift and parallel flows. One has:

$$\Gamma_{total}^{pol} = \left(2\gamma + M_o\right) n_o c_s \sin\theta \tag{51}$$

(Note that in this paper the symbol "Γ" denotes *flux density*, while "F" denotes *flux*.) The values of $\Gamma_{total}^{pol} = /\left(n_o c_s \sin\theta\right)$ are plotted in Fig.5. For the intuitive boundary condition of (a, b) = (0, 0) there is no dependence on the v_{pol}, γ. That is, the total sink action of the target is not affected by v_{pol} – at least when *normalized* by n_o (we have yet to bring in the fact that n_o itself depends on v_{pol}, γ and that does result in an asymmetric sink action). For other values of (a,b), however, even this normalized sink action is dependent on v_{pol}.

In order to bring in the dependence of n_o on γ, a, b from Eq. (50) we need to evaluate G. This is done by relating G to the total particle source in the flux tube, target-to-target, S_{total} [particles/m^2/s]. One has:

$$S_{total} = n_o^{out} c_s \left(2\gamma + M_o(\gamma, a, b)\right) + n_o^{in} c_s \left(-2\gamma + M_o(-\gamma, a, b)\right) \tag{52}$$

Thus:
$$G = c_s S_{total}\, f(\gamma, a, b) \tag{53}$$

where

$$f(\gamma,a,b) \equiv \left[\frac{\left(2\gamma + M_o(\gamma,a,b)\right)}{M_o(\gamma,a,b)\left(2\gamma + M_o(\gamma,a,b)\right) + 1} + \frac{\left(-2\gamma + M_o(-\gamma,a,b)\right)}{M_o(-\gamma,a,b)\left(-2\gamma + M_o(-\gamma,a,b)\right) + 1} \right]^{-1} \tag{54}$$

This function is shown in Fig. 6.

It is also useful to relate n_o to n_{max}, the maximum value of n in the flux tube – roughly midway between the targets and thus to be associated with the "top" or "midplane" or "edge-of-the-core" density. From Eq. (38) we have n(v). Differentiating we find:

$$n_{max} = \frac{G / c_s^2}{\left(1 - \gamma^2\right)} \tag{55}$$

Thus:
$$\frac{n_o}{n_{max}} = \frac{1 - \gamma^2}{M_o\left(2\gamma + M_o\right) + 1} \tag{56}$$

This relation is shown in Fig. 7. For the intuitive boundary condition, i.e., (a, b) = (0, 0), one finds that $n_o^{in}/n_{max} \to 0$ for $\gamma \to 1$, which is also true for most of the sets of values of (a, b), although not all. For the intuitive boundary condition, $n_o^{out}/n_{max} \to 1$ as $\gamma \to 1$. For most of the other sets of (a, b), one has $n_o^{out}/n_{max} \to 0$ as $\gamma \to 1$, indicating *detachment at both targets* for large $|\gamma|$, i.e., for strong poloidal drifts. (The cause of this effect can be seen from Fig. 6 where it may be noted that G only goes to zero at $\gamma = 1$ for (a, b) = (0, 0); from Eq. (55), one has $n_{max} \to \infty$ for $|\gamma| \to 1$, unless G also goes to zero there.) Whether or not this effect could be a cause of experimentally observed divertor detachment [19] depends on evaluating (a, b), obviously. In the interpretation of an experiment this can be done if sufficient experimental data are available to evaluate the radial scale lengths involved in (a, b), Eqs. (41)-(47). From the modelling view, one would have to solve the entire 2D system of SOL plus divertor plasma to establish (a, b). These ambitious undertakings are not attempted here. However, some further observations concerning the physical likelihood of finding cases, such as shown in Fig. 7, are given in the Appendix.

4. RADIAL $\vec{E}\times\vec{B}$ DRIFTS

The postulated flow pattern induced by the radial $\vec{E}\times\vec{B}$ drift is shown in Fig. 2. The flow along the SOL required to close this flux loop is simplified to slab geometry in Fig. 8. Assuming that E_θ is largest near the X-point, where the pitch angle is smallest and therefore poloidal T-gradients are often largest, then most of the influx to the SOL caused by v_r is near the inside end of the SOL flux tube, and most of the outflux (back into the core via v_r) is near the outside end of the SOL flux tube. In Fig. 8 we have simplified to the extreme of all influx at the inside end, all outflux at the outside end. Although $v_{||}$ will vary along the flux tube due (a) to the very fact that n varies (i.e., the effect we are trying to extract here), and (b) to the fact that the cross-sectional area of the flux tube varies poloidally (by a factor $\cong a/R$) – we will take here a constant value of $v_{||}$ as being representative of the magnitude of the induced parallel flow along the SOL.

The total out/in flux:

$$\phi \approx \frac{1}{2} 2\pi a \; 2\pi R \; n v_r \tag{57}$$

Assume this flux is carried by a SOL flux tube of thickness λ_{SOL}, thus:

$$\phi \approx 2\pi R (B_\theta / B) n v_{||} \lambda_{SOL} \tag{58}$$

Thus:

$$v_{||} \approx \frac{a\pi \, v_r}{(B_\theta / B)\, \lambda_{SOL}} \tag{59}$$

Taking:

$$v_r = \frac{E_{pol}}{B} = \frac{kT}{ea\pi B} \tag{60}$$

gives:

$$v_{||} = \frac{kT}{eB_\theta \, \lambda_{SOL}} \tag{61}$$

Example: T = 100 eV, $c_s = 10^5$ m/s, $B_\theta = 0.5$T, $\lambda_{SOL} = 10^{-2}$ m, one finds $v_{||} \cong 2\times10^4$ m/s which is significant compared with the sound speed. We therefore can anticipate significant drag on this SOL flow caused by shear viscosity (and perhaps by other processes such as neutral friction). For simplicity we assume here that the plasma just inside the LCFS is stagnant (it may actually be moving with or against the SOL flow, reducing or enhancing the shear viscous drag on the SOL flow). We also assume a no-slip condition at the LCFS. The shear stress acting on the SOL flow is then:

$$\tau = \mu_\perp \left.\frac{dv_{||}}{dr}\right|_{LCFS} \tag{62}$$

where we approximate

$$\left.\frac{dv_{||}}{dr}\right|_{LCFS} \approx \frac{v_{||}}{\delta} \tag{63}$$

where δ is the boundary layer shear viscosity thickness, given by the usual Reynolds expression:

$$\delta \approx \left(\frac{\mu_\perp L}{m n v_{||}}\right)^{1/2} \tag{64}$$

Thus:

$$\tau \approx \frac{\mu_\perp v_{||}}{\left(\frac{\mu_\perp L}{m n v_{||}}\right)^{1/2}} \tag{65}$$

In order for the SOL flow to close the loop a pressure drop Δp must exist along the SOL to balance the shear force, thus:

$$\tau L \approx \Delta p \, \lambda_{SOL} \tag{66}$$

Using

$$\mu_\perp = \alpha m n D_\perp \tag{67}$$

$$p = 2nkT \tag{68}$$

$$c_s^2 = 2kT/m \tag{69}$$

one obtains:

$$\frac{\Delta p}{p} = \frac{v_{||}}{c_s^2 \lambda_{SOL}} \left(\alpha v_{||} L D_\perp\right)^{1/2} \tag{70}$$

Example: T = 100 eV, $v_{||} = 2\times10^4$ m/s, $c_s = 10^5$ m/s, $\lambda_{SOL} = 10^{-2}$ m, $\alpha = 1$, L = 50 m, $D_\perp = 1$ m^2/s gives $\Delta p/p = 0.2$ from the inside to the outside.

Clearly, the foregoing is a rough estimate and all that can be concluded from it is that for reasonable assumptions about the edge parameters one can find $\Delta p = 0(p)$, i.e., there is a substantial pressure difference from inside to outside, due to flows induced by radial E×B drifts.

We consider next what effect in/out pressure differences would be expected to have on in/out recycling and temperature differences at the two divertor targets. We use here a modified Two-Point Model relating the "top" or "mid-plane" conditions, "top", to the target conditions "div". We define a pressure loss/gain factor f_p by:

$$n_{div}\, T_{div} \equiv f_p \frac{1}{2} n_{top}\, T_{top} \tag{71}$$

where the factor $\frac{1}{2}$ assumes that the parallel exit velocity at the targets is the sound speed (and we are assuming $v_{pol} = 0$ in this Section). For no v_r effect, $f_p = 1$. For $v_r \neq 0$ and "forward" $\vec{B}$, one has $f_p^{in} > 1$, $f_p^{out} < 1$ due to shear viscous, and other drag, on the SOL parallel flow induced by v_r.

From energy balance:

$$q_{\|}(1 - f_E) = \gamma n_{div}\, c_{s_{div}}\, kT_{div} \tag{72}$$

where $q_{\|}$ ≡ power flux density along the SOL into the divertor,

f_E ≡ fraction of that power flux which is radiated in the divertor associated with hydrogenic recycle, also impurities,

γ ≡ sheath transmission heat coefficient ≈ 7.

Combining (71) and (72) gives the divertor plasma temperature:

$$T_{div} = \frac{m}{2}\left[\frac{2q_{\|}(1-f_E)}{\gamma f_p n_{top}\, T_{top}}\right]^2 \tag{73}$$

One also has the particle target flux density $\Gamma_{o\|} = n_o c_{s_o}$. Thus:

$$\Gamma_{div_{\|}} = \frac{f_p^2 (n_{top})^2\, (T_{top})^2}{2m\, q_{\|}(1-f_E)} \tag{74}$$

For the high recycling divertor one has:

$$T_{top} \approx \left(\frac{7}{2}\frac{q_{\|}L}{\kappa_o}\right)^{2/7} \tag{75}$$

and so one can take the upstream condition, n_{top} and T_{top}, as being virtually fixed by the setting of the externally-controlled parameters of the tokamak. We thus see that the in/out asymmetries will be related to in/out differences in f_p and/or f_E.

At the inner target $f_p > 1$ and so $\Gamma_{div\parallel}$ goes up – indeed strongly (varying as f_p^2), i.e., recycling is stronger at the inner target than the outer. At the same time T_{div}^{inner} goes down, strongly (varying as f_p^{-2}) while T_{div}^{outer} goes up. Hydrogenic and impurity radiation losses generally increase at lower temperatures, and thus f_E^{inner} would be expected to increase. This further reduces T_{div}^{inner}, increases T_{div}^{inner}, again strongly, since square powers are involved. Thus a strong positive feedback exists which ultimately stabilizes through effects not considered here. Therefore, an initially small in/out pressure asymmetry can – *for high recycling conditions* – result in large in/out temperature and recycling differences.

(It is worth noting that in Section 3, on poloidal drifts, we assumed *isothermal* conditions – as is appropriate for the low recycling regime where poloidal E×B drifts are likely to be more important than radial E×B drifts. Thus the high recycle relations, Eqs. (73)-(75), do not apply in that case, and one would not expect to see the strong multiplying effects noted above for the radial E×B drift case.)

It should also be noted that it has *not* been assumed that an in/out asymmetry exists in the total *power* going into the inner and outer divertor "legs". The asymmetry considered here would only manifest itself, as to power, in the *split* between divertor radiation and heat deposition on the target. There may indeed be an in/out asymmetry in the total power into the two divertor legs, due to E×B radial drifts – provided the convected power associated with the E×B, v_r drift is significant compared with the anomalous (fluctuation-driven) conduction and convection; this situation was the one treated by Hinton and Staebler [3]. (The diamagnetic drifts cannot influence in/out power flows [1] as they are largely divergence-free.) Experimentally, it appears that there is often little or no in/out asymmetry in the total power into the 2 divertor legs [20], evidently indicating that the convected heat flux associated with E×B v_r may often be small compared with anomalous heat fluxes. In such cases, the most important effect of the radial E×B flows on power relate to the split between divertor radiation and target heating.

5. DISCUSSION AND CONCLUSIONS

Under operating conditions where the temperature varies little along the SOL, for example, "low recycling conditions", also when the parallel power flow is very high, E×B poloidal drifts are more important than E×B radial drifts. Making then an isothermal assumption, and employing the modified Bohm-Chodura Criterion for the parallel flow velocity at the targets [2] (i.e., modified to account for poloidal E×B drifts), solutions were found for the variation

of plasma density (thus pressure) between the inner and outer targets of a single null divertor. When v_{pol}/c_s is large enough, the in/out asymmetry – which gives the highest n, p at the outer target for $\vec{B}$ in the "forward" direction – can be quite substantial, even corresponding to essentially "detached" conditions at the inner target. It is conceivable that simultaneous detachment could occur at both targets by this mechanism, however, it would seem improbable due to the following factors:

(a) detachment is usually associated with high density ($\bar{n}_e$) operation [19], where the "high recycling" regime is expected and where, therefore, poloidal E×B drifts would be expected to be less important than radial E×B drifts.

(b) rather unusual cross-field variations (governing the a, b factors in the drift-corrected Bohm-Chodura Criterion [2]) of density, temperature, and/or normalized sheath potential drop are required. It remains to be demonstrated that such variations can exist self-consistently by carrying out a complete 2-D numerical code analysis, including the two divertor plasmas, the rest of the SOL and the drift-corrected boundary conditions [2].

(c) It remains to be demonstrated (by the same method as (b), above) that a physically acceptable solution, avoiding singularities in the middle of the flow, can exist for such unusual values of a, b.

In high recycling "operation" – or to be more accurate – "the well-insulated divertor" regime, where parallel temperature gradients are substantial – the radial E×B drift will be more important, and, for the "forward" direction of $\vec{B}$, will give the highest pressure at the *inside* target. A simple analysis has been made for this case, assuming no *direct* interaction of the parallel SOL flow induced by the E×B v_r drift and the ionization-recycling zones at each target (i.e., no co-mingling of these flows). An in/out pressure difference arises associated with the viscous shear drag on the v_r-induced parallel flow. This *indirectly* influences the recycle fluxes at each target since they are strongly influenced by the local pressure. In this way higher recycling fluxes and lower plasma temperatures are expected at the inner target in this regime.

If this v_r-induced effect becomes strong enough then T_e^{inner} could drop so low that a completely separate process leading to detachment could take over, and actually *reduce* the plasma pressure very close to the inner target: the separate process referred to is that associated with momentum loss by the ions flowing to the inner target, due to friction with recycling neutrals [21]. By itself, such a decrease in f_p would tend to *raise* T_e, see Eq. (73),

thus turning off the effect; however, the increased radiative losses, if strong enough (f_E large, see Eq. (73)), can compensate for this. We thus have a somewhat complicated possible relation between E×B radial drifts and detachment: if v_r/c_s is not too large then the inner target (for "forward" $\vec{B}$) will be strongly attached with plasma pressure and recycling higher than at the outer target; if v_r/c_s is large then the inner divertor could detach due to neutral friction effects; at the same time the pressure at the outer target could go to very low values and *also* "detach", in a different sense. This latter detachment, however, would not necessarily be associated with particularly low values of T_e^{outer}, since low values for f_p, see Eq. (73), tend to make T_e rather large. Therefore, there could be "detachment" simultaneously at both targets, associated with a strong E×B radial drift, however, the fundamental cause of the detachment would be different at each target: at the outer target it would be directly due to reduction in plasma pressure caused by the E×B radial drift; at the inner target it would be due to neutral friction. One would therefore expect to see rather different plasma conditions at inner and outer targets, when simultaneous detachment occurs, and for these conditions to reverse when the direction of $\vec{B}$ is reversed. On JET relatively little difference is seen, experimentally, between the conditions at the two detached targets and the changes with change of $\vec{B}$ are also moderate [19]. It thus would not seem that radial E×B drift effects are usually strong enough to play a major role in detachment (simultaneously detachment at both targets). It may be that these drifts do play a role in cases where detachment occurs just at the inside. It would appear that a more common situation would be where these drifts just cause high recycling, and low T_e at the inner target, rather than actual detachment.

The electrical biasing of divertors provides a separate category of information on the effect of drifts. The Tokamak de Varennes can be operated with electrical biasing of the divertor plates such as to permit external manipulation of the radial electric field in the SOL [22]. The resulting poloidal drifts lead to measured pressure asymmetries [22] between the two divertors, which are consistent with the analysis of Section II. At the same time, the measured parallel drift velocity in the SOL [23], as measured with a special, "Gundestrup" probe, is also in the expected direction, i.e., opposite to the direction of the poloidal drift. It would appear that these E_r-induced pressure asymmetries and parallel flow patterns are explicable in terms of the simple concepts employed in Section II and by Cohen and Ryutov [16]. It is not evident that it is necessary to analyse the relationship between the radial electric field and the radial current [24, 25] in order to interpret these asymmetries and flows, since *measurements* of E_r can be made. Of course, if one seeks a complete, predictive theory then the relation between E_r and j_r has to be identified.

ACKNOWLEDGMENTS

The authors wish to thank Peter Harbour and Gary Staebler for helpful discussions.

P. C. Stangeby acknowledges support by the Canadian Fusion Fuels Technology Project.

APPENDIX

THE PHYSICAL LIKELIHOOD OF THE SOLUTIONS IN SECTION 3, FIG. 7

It should be noted that the results of Section II, culminating in the examples shown in Fig. 7, have been based solely on evaluating n, from Eq. (38), at the 2 end points. It is worthwhile to consider whether or not the v(y) and n(y) solutions make sense for values of y *between* the two targets.

From Section II one can show:

$$\frac{dv}{dy} = \frac{S_{iz}\left[v^2 + c_s^2 - 2c_s\gamma v\right]^2}{G \sin\theta\left(c_s^2 - v^2\right)} \qquad (A.1)$$

Generally $v_o^{in} < 0$ and $v_o^{out} > 0$. Thus we need to consider under what circumstances $\frac{dv}{dy} > 0$. For some sets of (γ, a, b) it is readily established that $\left|v_o^{in}\right| > c_s$ (for $\vec{B}$ "forward"). In such cases one would not have dv/dy > 0 near the inner target unless S_{iz} is negative, i.e., there is net sink action in that region, related to cross-field ("anomalous") flows or recombination. The physical likelihood of this happening would have to be considered; it would certainly seem to be an odd situation. For some of the (a, b) sets this problem does not arise; for the "intuitive" case, (a, b) = (0, 0), for example, $v_o^{in} = -c_s$, $v_o^{out} = +c_s$ and so assuming $S_{iz}(y) > 0$ for all y > 0 gives dv/dy > 0.

One also notes from Eq. (A.1) that a potential problem arises if $v \rightarrow c_s$ at some point between the two plates. Again, it is readily shown that $|v| > c_s$ for some sets of (γ, a, b); for example, for (γ, a, b) = (1/2, 0, -1), one has v_o^{in} = -0.62 c_s, v_o^{out} = +1.62 c_s. One can only avoid unphysical singularities in the midst of the SOL if S_{iz} switches sign at the sonic transition. Again one must consider how likely it is that one would encounter such a situation.

In the present context one can only speak of "likelihood" of encountering certain spatial distributions, $S_{iz}(y)$, since we are not solving the complete 2D SOL system. It should also be noted that in Section II we are only considering a highly simplified situation. We have assumed:

(i) v_{pol} constant along the SOL,

(ii) $T_{e,i}$ constant along the SOL,

(iii) ($|\gamma|$, a, b) the same at each target,

(iv) the boundary condition in the *marginal* form.

(It is common practice to use the marginal form of the Bohm-Chodura Criterion, $v_{exit} = c_s$ (for no drifts); supersonic exit velocities are also permitted [26] and should therefore be allowed for in modelling.)

When these highly constraining assumptions are relaxed, as one can do in 2D numerical code modelling of the SOL, then other, more physically likely processes, can give $dv/dy > 0$ (and can avoid $dv/dy \rightarrow \infty$) than requiring S_{iz} to change sign. For example, when T-gradients are present, smooth sonic transitions are readily achieved [27, 28].

What, then, are we to make of the results drawn in Fig. 7? One can say that – even within the context of the simplifying, and rather unphysical assumptions that we have had to make here in order to achieve analytic results – these solutions are not *impossible* ones – although most of them are *unlikely*. (The "intuitive" case, (a, b) = (0, 0), is not subject to this criticism, nor are some other sets of (γ, a, b).) If one were to relax the simplifying assumptions then it may be – although this remains to be demonstrated – that solutions similar to those shown in Fig. 7 would be naturally generated (only "similar" because the solutions of Fig.7 are explicitly for v_{pol}, $T_{e,i}$ constant along the SOL, etc.).

Therefore, on the specific issue of whether or not poloidal drifts could explain simultaneous detachment at both divertor targets – i.e., solutions similar to (γ, a, b) = (1, 0, -1), say – this can probably only be established by using 2D numerical code modelling of the SOL [10, 11], with boundary conditions as from [2]. However, since detachment is associated with high (upstream) density, when one expects radial drifts to be more important than poloidal ones – it would not seem likely that poloidal drifts would be the cause of simultaneous detachment at both targets, as is often observed experimentally [19].

REFERENCES

[1] A. V. Chankin and P. C. Stangeby, *Plasma Phys. Control. Fusion* **36** (1994) 1485.

[2] P. C. Stangeby and A. V. Chankin, *Phys. of Plasmas,* **2** (1995) 707.

[3] F. L. Hinton and G. M. Staebler, *Nucl. Fusion* **29** (1989), 405.

[4] A. Nedospasov and M. Tokar, *Proc. XIIth EPS Conf.,* Aachen, 1983.

[5] P. J. Harbour, et al, *J. Nucl. Mater.* **128, 129** (1984), 359.

[6] P. Cooke and A. Prinja, *Nucl. Fusion* **27** (1987) 1165.

[7] J. Neuhauser and R. Wunderlich, *J. Nucl. Mater.* **145-147** (1987) 877.

[8] G. P. Maddison, D. Reiter, P. C. Stangeby, A. K. Prinja, *Proc. 20th EPS Conf.,* Lisboa, 1993, Pt. II, p. 779.

[9] P. J. Harbour, private communication, JET, 1995.

[10] G. M. Staebler, *Nucl. Fusion* **31** (1991) 729.

[11] M. Baelmans, D. Reiter, R. R. Weynants, R. Schneider, *J. Nucl. Mater.* 1995, in press.

[12] A. V. Chankin, S. Clement, S. K. Erents, et al, *Plasma Phys. Control. Fusion* **36** (1994) 1853.

[13] P. J. Harbour, *Contrib. Plasma Phys.* **28** (1988) 417.

[14] A. V. Chankin, S. Clement, L. deKock, et al, *J. Nucl. Mater.* **196-198** (1992) 739.

[15] G. D. Hobbs and J. A. Wesson, *Plasma Phys.* **9** (1967) 85.

[16] R. H. Cohen, D. Ryutov, Comments on *Plasma Physics and Controlled Fusion* **35** (1993) 1271.

[17] M. Tendler and V. Rozhansky, *Comments Plasma Phys. Controlled Fusion* **13** (1990), 191.

[18] S. I. Krasheninnikov, D. J. Sigmar and P. N. Yushmanov, submitted *Phys. Plasmas.*

[19] G. F. Matthews, *J. Nucl. Mater.* 1995, in press.

[20] N. Asakura, N. Hosogane, K. Itami, et al, *Proc. 15th Int. Conf. Plasma Phys. and Controlled Fusion Research,* Seville, Spain, Sept. 26 - Oct. 1, 1994, IAEA-CN-60/A-4-I-3.

[21] P. C. Stangeby, *Nucl. Fusion* **33** (1993) 1695.

[22] R. Décoste, J.-L. Lachambre, G. Abel, et al, *Phys. Plasmas* **1** (1994) 1497.

[23] C. S. MacLatchy, C. Boucher, D. A. Poirier, et al, *J. Nucl. Mater.* **196-198** (1992) 248.

[24] V. Rozhansky and M. Tendler, *Phys. Plasmas* **1** (1994) 2711.

[25] G. M. Staebler, *J. Nucl. Mater.,* in press.

[26] P. C. Stangeby, *Phys. of Plasmas,* March 1995, in press.

[27] R. Chodura, NATO Summer School, 1984.

[28] P. C. Stangeby, *Plasma Phys. Control. Fusion* **33** (1991) 671.

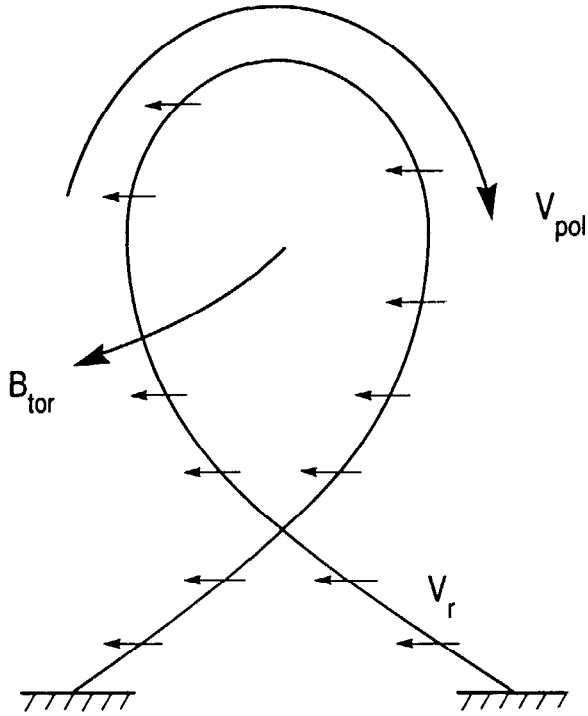

Fig.1: The outer divertor target is on the right. The "forward" direction of $\vec{B}$ *is shown, giving the ion* $\vec{\nabla}B$ *drift toward the divertor. The resulting* $\vec{E}\times\vec{B}$ *poloidal drift,* v_{pol}*, and radial,* v_r*, directions are shown for the usual case of the radial electric field pointing outward in the SOL, and the poloidal electric field pointing toward the targets in the SOL. Both* v_{pol} *and* v_r *are reversed when the toroidal field is reversed.*

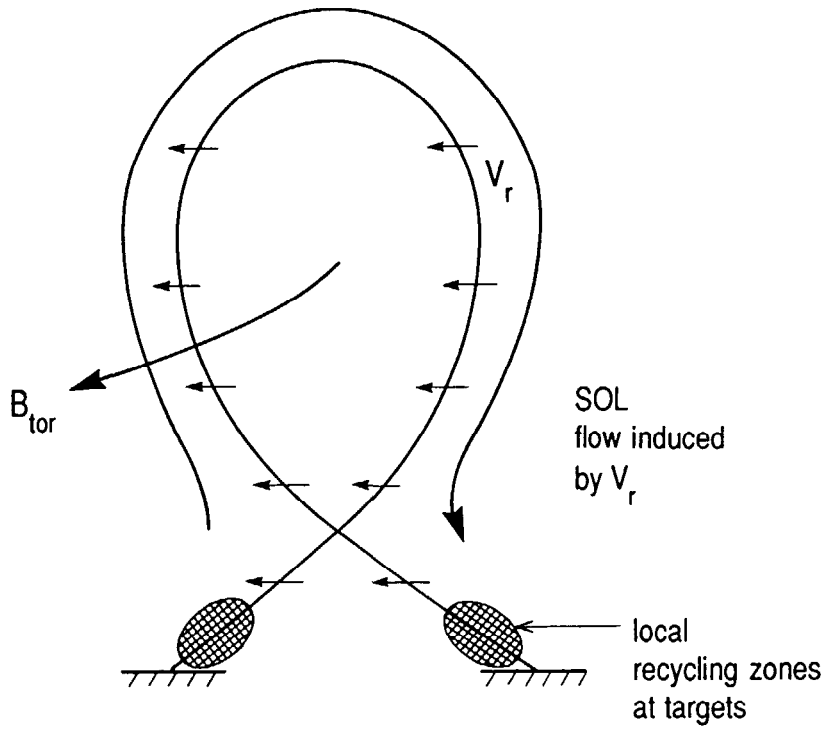

Fig.2: For the situation where the poloidal $\vec{E}\times\vec{B}$ *drift can be neglected compared with the radial* $\vec{E}\times\vec{B}$ *drift, a return flow is induced along the SOL, from inside to outside target regions ("forward" direction of* $\vec{B}$ *assumed). Here it is also assumed for simplicity that the local recycling zones at each target are very close to each target, and thus the two types of parallel flow (*v_r*-induced, and ionization-induced) do not directly interact, i.e. do not "co-mingle".*

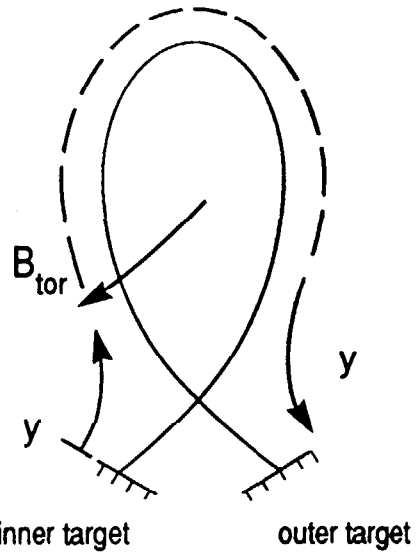

Poloidal Plane:

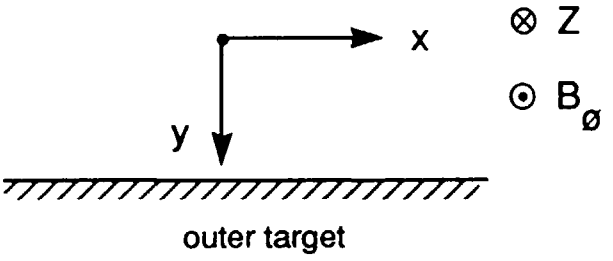

Toroidal View:

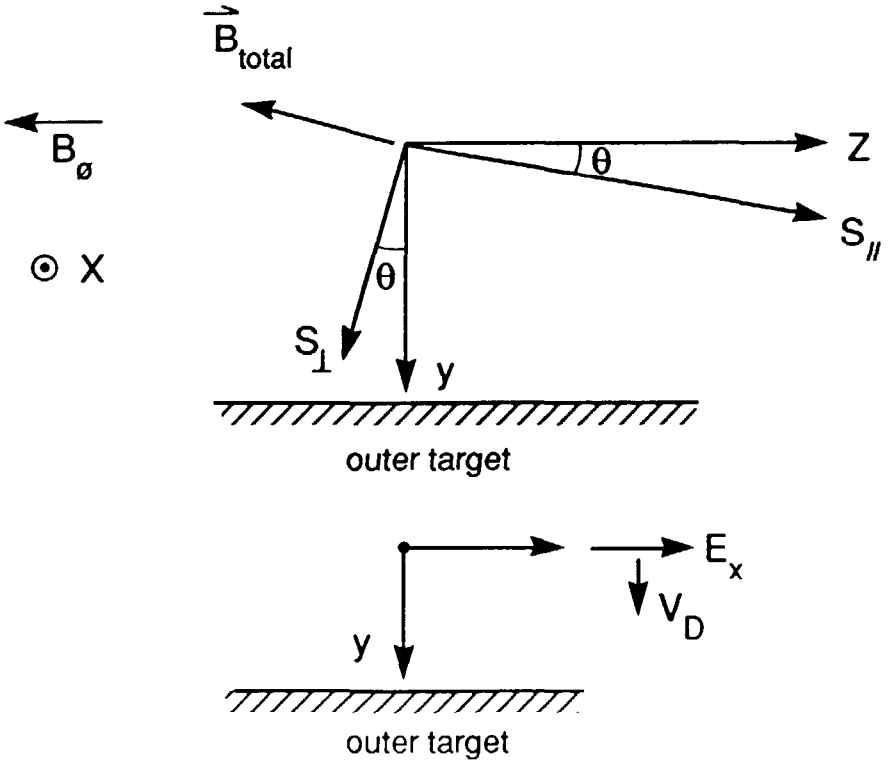

Fig.3: The coordinate system for analysis of the poloidal E×B drift case, Sec.3.

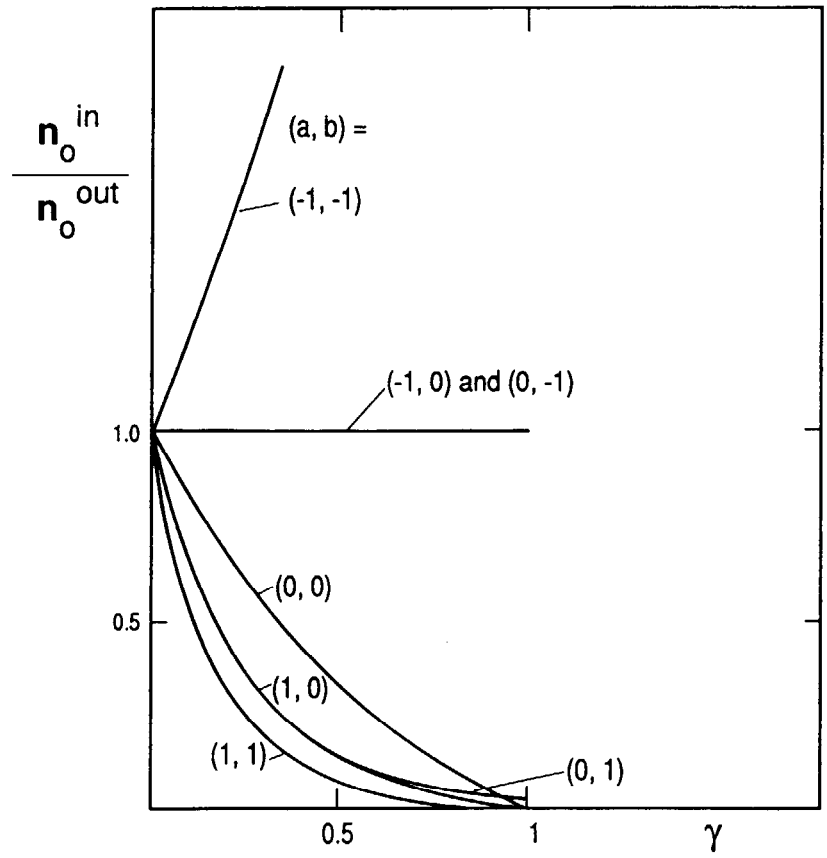

Fig.4: For the case of poloidal $\vec{E}\times\vec{B}$ drift, Sec.3, the in/out density ratio at the targets (thus, also the pressure ratio since isothermal conditions are assumed). $\gamma \equiv v_{pol}/(2c_s \tan\theta)$ gives the strength of the poloidal drift. Parameters (a,b) are given by ratios of radial e-folding lengths in the SOL, see Sec.3. For the simplest, "intuitive" boundary condition case, (a,b)=(0,0), the effect of the poloidal drift is to reduce/raise the inner/outer plasma density.

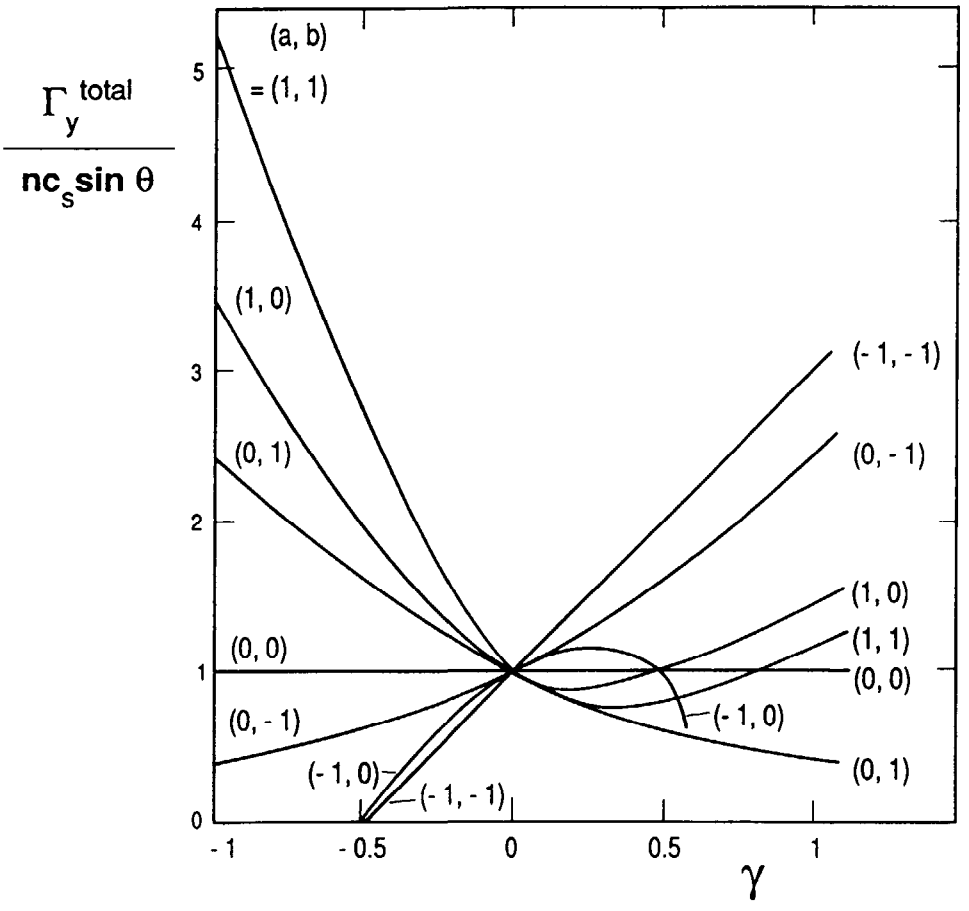

Fig.5: For the case of poloidal $\vec{E}\times\vec{B}$ *drift, Sec.3, the total particle outflux density (due to both parallel flow and cross-field drift) to the targets. [Note that, here, this outflux has been normalized by* $nc_s \sin\theta$*, therefore, the fact that n itself changes with* γ*, Fig.4, has not been folded in yet.]* $\gamma = v_{pol}/(2c_s \tan\theta)$ *gives the strength of the poloidal drift. Parameters (a,b) are given by the ratios of radial e-folding lengths in the SOL, see Sec.3. For the simplest, "intuitive" boundary condition case, (a,b)=(0,0), the poloidal drift has no effect on this* normalized *total outflux, since the change in parallel flux is exactly compensated by the change in cross-field flux.*

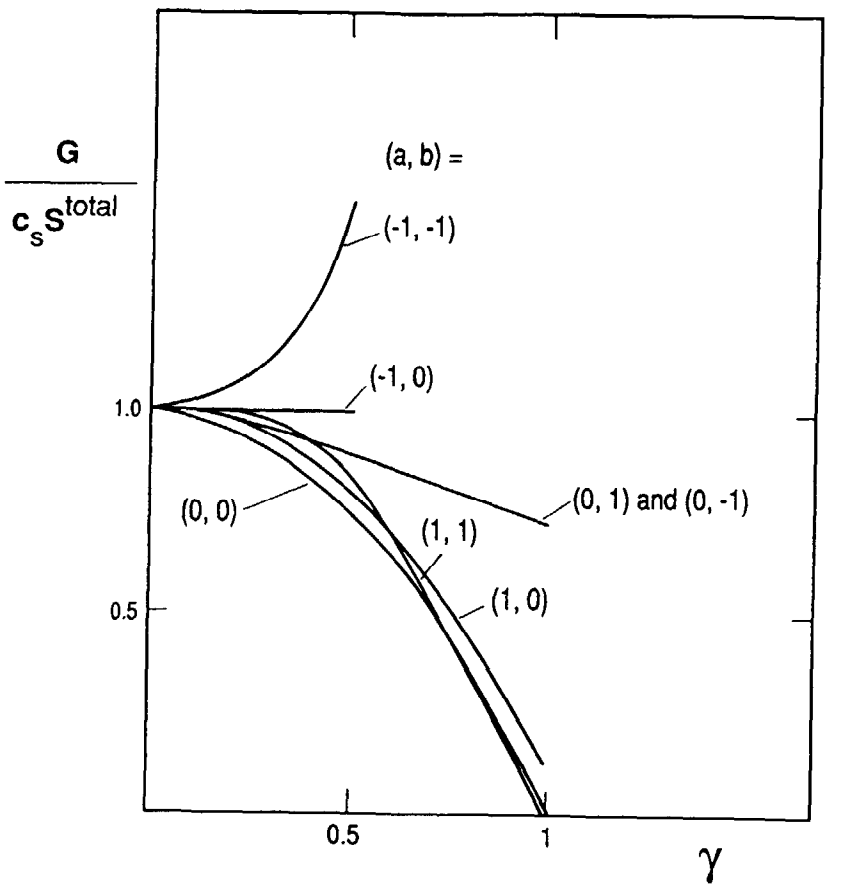

Fig.6: The case of poloidal $\vec{E}\times\vec{B}$ *drift, Sec.3. The factor* $G(\gamma, a, b)$ *required in Eq.(50) to give the plasma density at the target.* c_s *= sound speed,* S^{total} *= total particle source rate in the flux tube, target-to-target. For parameters* γ, *a, b, see Figs.4 and 5.*

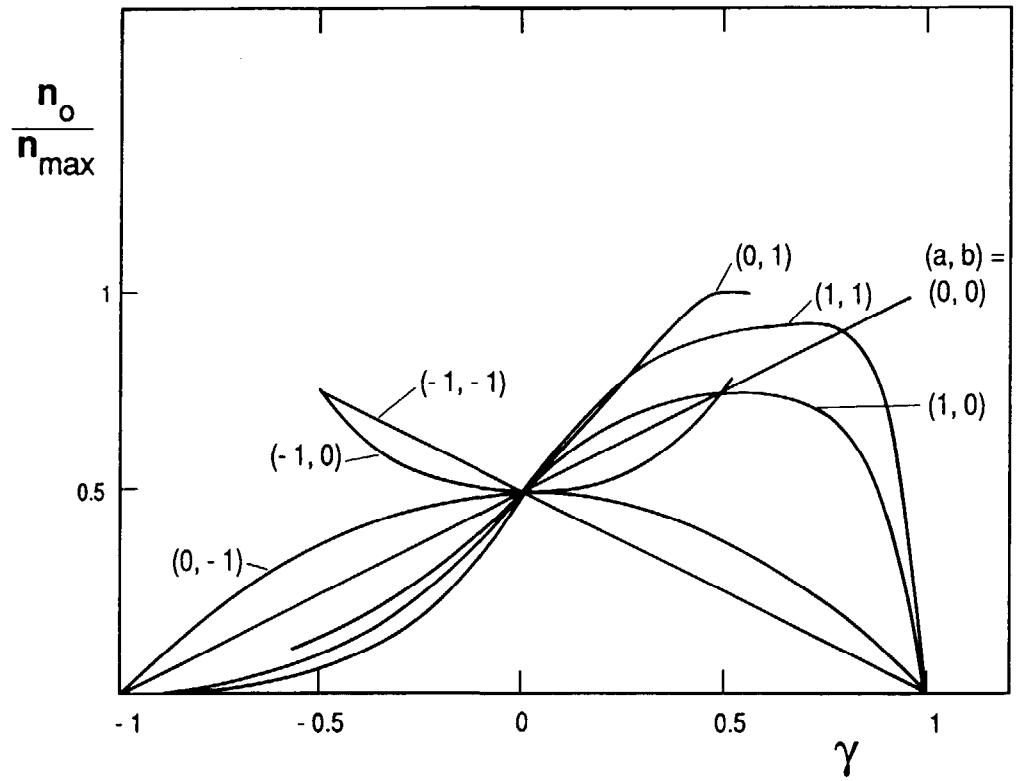

Fig.7: The case of poloidal $\vec{E}\times\vec{B}$ drift, Sec.3. The density at the target normalized by the maximum density along the SOL, i.e. approximately the value at the mid-point between targets. $\gamma=v_{pol}/(2c_s \tan\theta)$ gives the strength of the poloidal drift. Parameters (a,b) are given by the ratios of radial e-folding lengths in the SOL, see Sec.3. For the simplest, "intuitive" boundary condition, (a,b)=(0,0), the plasma completely detaches at the inner target for sufficiently strong poloidal drift (γ=-1), while remaining strongly attached at the outer target ("forward" direction of $\vec{B}$ assumed).

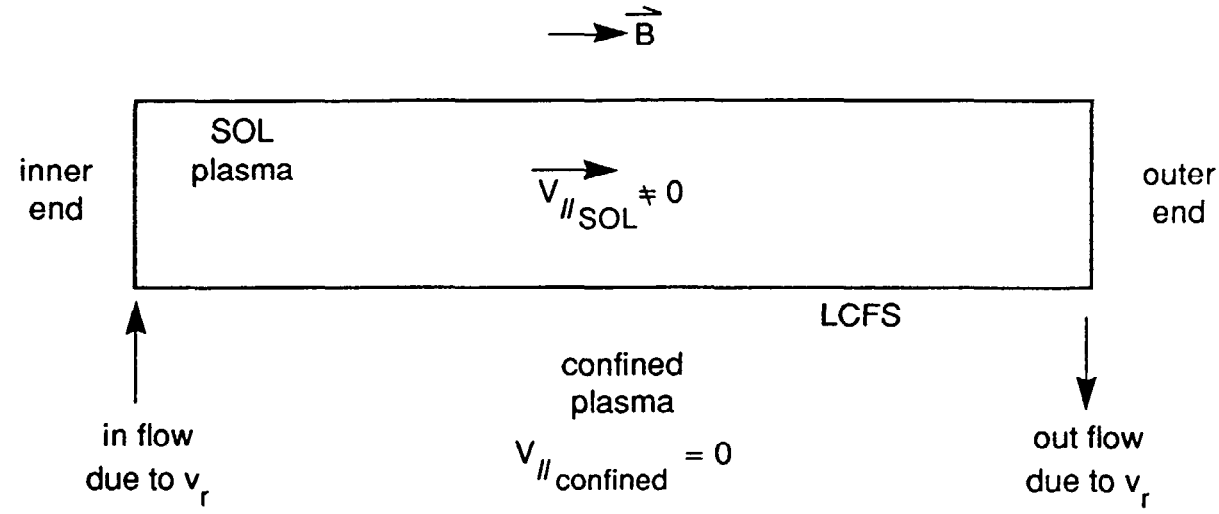

Fig.8: For the case of radial $\vec{E}\times\vec{B}$ drift, Sec.4. The SOL has been straightened out. The wall is on the top side; the confined plasma is on the bottom side. The parallel return flow, $v_{||SOL}$, is induced by the radial $\vec{E}\times\vec{B}$ flux which, here, is taken to enter the SOL near the inner target, and to exit back to the confined plasma at the outer end. This induced parallel flow generally suffers frictional loss, thus making the plasma pressure at the inner target higher than at the outer target – the opposite effect to the poloidal drift.